ELSEVIER

Journal of Hazardous Materials B129 (2006) 151–157

Journal of Hazardous Materials

www.elsevier.com/locate/jhazmat

Hydrothermal treatment of bottom ash from the incineration of municipal solid waste: Retention of Cs(I), Cd(II), Pb(II) and Cr(III)

Raúl Peña, Ana Guerrero, Sara Goñi *

Institute of Construction Science Eduardo Torroja (CSIC), C/Serrrano Galvache, 4, 28033 Madrid, Spain

Received 24 May 2005; received in revised form 11 August 2005; accepted 20 August 2005
Available online 27 September 2005

Abstract

The retention of Cs^+, Cd^{2+}, Pb^{2+} and Cr^{3+} by the compounds formed as a result of the hydrothermal treatment of the bottom ash from the fluidized-bed incineration of municipal solid wastes is examined in this work. The amount of Cs^+ retained and the distribution coefficient, K_d, were considerably lower than those for Cd^{2+}, Pb^{2+} and Cr^{3+}, independently of the type of compounds formed by the different bottom ash treatments. The high percentage of Cs^+ retained (31%), with a K_d of 222 ml/g, occurred after treatment of the bottom ash in NaOH at 200 °C, where zeolite-type A ($Na_6[AlSiO_4]_6{\cdot}4H_2O$) was the major compound, together with aluminum tobermorite ($Ca_5Si_5Al(OH)O_{17}{\cdot}5H_2O$). In the case of Cd^{2+}, Pb^{2+} and Cr^{3+}, the amount retained was ∼99% under all of the conditions studied.

Keywords: Bottom ash; Incineration of municipal solid waste; Metals retention waste disposal; Hydrothermal treatment

1. Introduction

The present work is part of an extensive investigation conducted in our laboratory and related to a search for treatments of ash generated from municipal solid waste incineration (MSWI) that would increase the potential applications of the ash. The main applications for bottom ash from MSWI are in the construction field [1–5]. However, expansion produced by hydrogen (from metallic aluminum dissolution) and a high chloride content are serious problems for these wastes and must be treated before the ash is used in construction [6–8]. Moreover, MSW incineration residues contain elements, such as calcium, silicon, aluminum and sulfur, which can be used as secondary raw materials for special cements containing hydraulic materials, such as sulfo-belite [9,10], alinite [11,12] and portland cement, after the incinerated ash has been desalinized by washing with water [13,14].

Aluminum-substituted tobermorite and different types of zeolites were synthesized previously from hydrothermal treatment (HT) in an NaOH solution of fly ash from MSWI [15–18]. In these works, the fly ash was pretreated by repeated water-washing and heating at 800 °C [15], acid treatment and water-washing [16], or mixing with different types of additions, such as amorphous aluminum silicate and glass powder [17] or aluminum and silica [18]. However, no prior work has been found on the use of bottom ash from the fluidized-bed combustion of MSW, instead of fly ash, and without the extra addition of other components, for synthesizing, via HT, compounds with immobilization capacity.

Bottom ash from the fluidised-bed combustion of MSW contains, among other things, a great amount of silica from the sand of the fluidized bed, which could be re-used in other processes. In a previous work [19], we studied the transformation of bottom ash as a function of various types of HT in NaOH and water, at temperatures ranging from ambient to 200 °C. The results showed that bottom ash was transformed in compounds with potential immobilization capacity, such as zeolite-type A ($Na_6[AlSiO_4]_6{\cdot}4H_2O$), aluminum tobermorite ($Ca_5Si_5Al(OH)O_{17}{\cdot}5H_2O$), andradite ($Ca_3Fe_2(SiO_4)_{3-x}(OH)_{4-x}$), $Ca_3AlFe(SiO_4)(OH)_8$, ettringite ($Ca_6Al_2(SO_4)_3(OH)_{12}{\cdot}26H_2O$), katoite ($Ca_3Al_2(SiO_4)(OH)_8$), α-$C_2SH$ (α-$Ca_2SiO_4{\cdot}H_2O$) and C–S–H gel ($Ca_{1.5}SiO_{3.5}{\cdot}xH_2O$).

The present paper focuses on the retention of Cs^+, Cd^{2+}, Pb^{2+} and Cr^{3+} by the aforementioned compounds previously synthesized by Peña et al. [19], which would represent a new application of bottom ash in environmental waste disposal. The

* Corresponding author. Tel.: +34 91 3020440; fax: +34 91 3020700.
E-mail address: sgoni@ietcc.csic.es (S. Goñi).

0304-3894/$ – see front matter © 2005 Elsevier B.V. All rights reserved.
doi:10.1016/j.jhazmat.2005.08.024

Table 1
Chemical composition of starting bottom ash (R1) (% by weight)

LOI	4.6
IR	5.2
SiO_2	34.1
Al_2O_3	19.3
Fe_2O_3	6.6
CaO	21.9
MgO	2.6
SO_3	3.3
Na_2O	2.1
K_2O	1.9
Cl^-	3.6
Zn	0.44
Cd	0.0013
Pb	0.13
Cr	0.032

LOI is loss on ignition at 1100 °C; IR is insoluble residue.

changes in the micro porosity, specific surface (BET-N_2) and microstructure of the bottom ash are also discussed.

2. Experimental procedure

Bottom ash was collected from the MSW incinerator (fluidized-bed combustion) of Valdemingómez, which is located in Madrid, Spain. The sampling was conducted four times (15 kg each time) during a month, then 1 kg portions of each of the four samplings were mixed to produce a more representative and homogeneous sample, denoted "R1."

The chemical composition and grain size distribution of the bottom ash (R1) are given in Tables 1 and 2, respectively. The chemical composition was determined according to the Spanish standard UNE-EN 196-2. The concentration of sand from the fluidized bed (quartz, SiO_2) of the bottom ash was 13.5% (determined according to the Spanish standard UNE 80-225-93). X-ray diffractometry (Fig. 1(a)) indicated the following crystalline compounds: SiO_2 (α-quartz), $Ca_2Al_2SiO_7$ (gehlenite), γ-$CaSO_4$ (soluble anhydrite), NaCl (halite), KCl (sylvite), α′L-Ca_2SiO_4, $CaCO_3$ (calcite) and metallic aluminum. The minority crystalline phases were α-Fe_2O_3 (hematite) and probably, Mg_2C_3.

Table 2
Grain size percentage distribution of bottom ash determined by laser spectrophotometer

	Grain size (μm)			Average size (μm)	BET surface area (m^2/g)
	<32	32 > x < 45	>45		
Bottom ash	44.0	14.5	41.5	37.2	0.798

Samples with potential adsorption or cation exchange properties, obtained previously from the transformation of the bottom ash after various treatments [19], were characterized by X-ray diffractometry (XRD), scanning electron microscopy (SEM) and energy-dispersive X-ray analysis. The surface areas and pore size distribution were measured by a multipoint Brunauer-Emmett-Teller (BET) method. The grain size distribution of bottom ash was measured by laser, with a spectrophotometer Láser Cilas Alcatel model 715. Isopropilic alcohol was used as dispersant.

XRD patterns were recorded on a diffractometer (Model PW 1730, Philips Electronic Instruments Co., Mahwah, NJ) and graphite monochromator with Cu $K\alpha_1$ radiation, and SEM analysis was performed with an Jeol 5400 instrument equipped with an energy-dispersive X-ray spectroscopy module (EDS) Oxford ISIS model. Metallized samples were prepared with carbon sputtering. SEM/EDX semiquantitative analyses were made at 20 kV

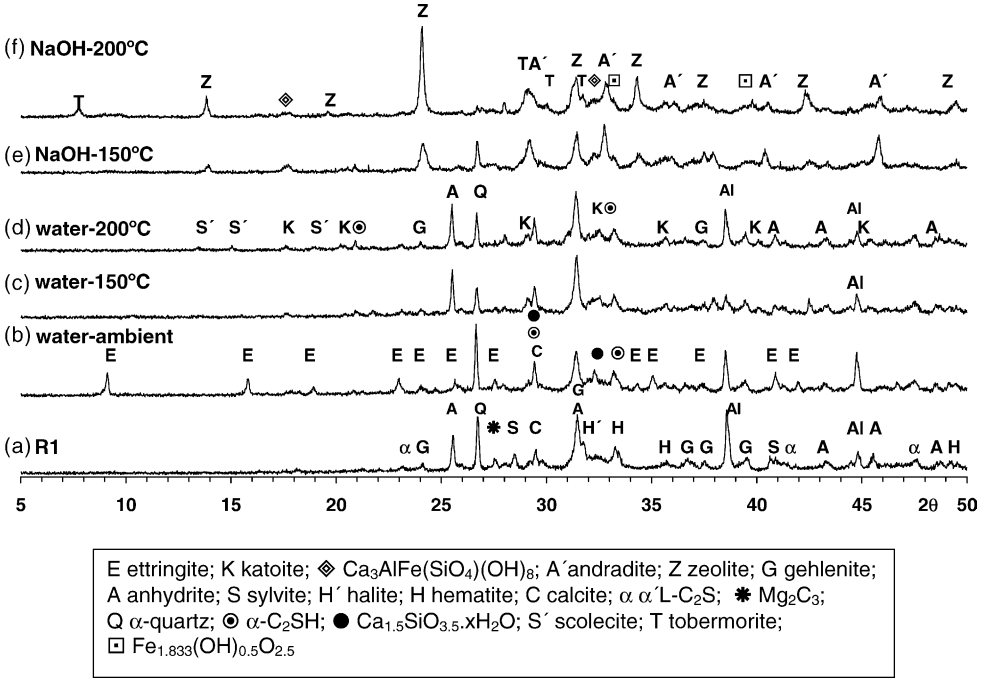

Fig. 1. Evolution of the X-ray diffraction pattern of bottom ash from MSWI as a result of the different treatments.

and a reference current of 300 μA on powder samples for determining the alkaline, alkaline-earth: iron oxides, alumina, silica and sulphur content. The EDX microanalysis have been carried out in spot mode over each different crystalline phase, being the limit detection of 0.2%. Surface area measurements were made by the BET multipoint method (Model ASAP 2010, Micromeritics Instrument Corp., Norcross, GA), using the previous degasification sample, at 50 °C during 24 h at 0.05 μmHg pressure, with N_2 gas as the absorptive. The surface areas were calculated from the isotherm data, using the BET equation, in the relative pressure range of 0.003–0.3. Pore size distributions were calculated according to the Barret-Joyner-Halenda (BJH) method.

Cs, Cd, Pb and Cr retention was measured in the selected samples, which were washed three times with demineralized water following the procedure described by Ma et al. [20]. The 25 ml of 0.02N NaCl containing 0.0002N $Cs^+/Cd^{2+}/Pb^{2+}/Cr^{3+}$ were added to 50 mg of each selected sample. The mixture was equilibrated for 24 h at 25 °C. Duplicates were prepared for each sample. After equilibration, the solids and solutions were separated. Blanks were prepared by using similar solutions and conditions but without the solid samples; the blank solutions were analyzed and the resulting concentrations taken as reference values. Analytical reagent grade CsCl, $CdCl_2$, $Pb(NO_3)_2$ and $CrCl_3{\cdot}6H_2O$ were used to prepare the solutions. Cesium, cadmium, lead and chromium were analyzed in solution on a Perkin-Elmer AANALYST-100 atomic absorption spectrometer.

3. Results and discussion

3.1. Characterization of phases selected for retention study

3.1.1. X-ray diffraction

For the retention study, we selected those phases obtained previously from the transformation of the bottom ash, after various treatments and which could have potential adsorption or cation exchange properties. The corresponding XRD patterns appear in Fig. 1. More characterization details are given elsewhere [19]. As shown in Fig. 1, the major transformation of the bottom ash was produced under HT in NaOH. At 150 °C (Fig. 1(e)), zeolite-type A ($Na_6[AlSiO_4]_6{\cdot}4H_2O$), andradite ($Ca_3Fe_2(SiO_4)_{3-x}(OH)_{4-x}$), together with $Ca_3AlFe(SiO_4)(OH)_8$, began to appear. At 200 °C (Fig. 1(f)), the bottom ash was fully transformed into massive zeolite-type A ($Na_6[AlSiO_4]_6{\cdot}4H_2O$), together with aluminum tobermorite ($Ca_5Si_5Al(OH)O_{17}{\cdot}5H_2O$), whereas andradite and $Ca_3AlFe(SiO_4)(OH)_8$ had decreased.

Under equivalent HT in water at 150 and 200 °C (Fig. 1(c and d)), small amounts of katoite, ($Ca_3Al_2(SiO_4)(OH)_8$), α-C_2SH (α-$Ca_2SiO_4{\cdot}H_2O$), C–S–H gel ($Ca_{1.5}SiO_{3.5}{\cdot}xH_2O$) and $CaAl_2Si_3O_{10}{\cdot}3H_2O$ zeolite-structure-type scolecite formed; anhydrite, gehlenite ($Ca_2Al_2SiO_7$) and SiO_2 (α-quartz) from the fluidized bed remained almost unchanged. Ettringite ($Ca_6Al_2(SO_4)_3(OH)_{12}{\cdot}26H_2O$) appeared when the bottom ash was treated at room temperature in water for 24 h (Fig. 1(b)).

3.1.2. Pore structures

According to the adsorption BJH method, Fig. 2 shows the transformation of the pore volume distribution of the bottom ash as a function of pore size in the mesopore and low macropore size range. As shown, the total porosity of the bottom ash (cumulative pore volume curve) increased by 1 order of magnitude as a result of HT in NaOH (from 0.0044 to 0.046 and 0.049 cm^3/g at 150 and 200 °C, respectively). When HT was in water, the porosity increased by 5.5 and 7 times at 150 and 200 °C, respectively. With treatment in water at room temperature, the porosity increased 5.3 times.

A wide peak centered at 12 nm was produced in the differential pore size distribution in all cases, which indicates a much higher proportion of pore volume in pores having diameters of ∼12 nm. The high intensity of the peak corresponds to HT in NaOH. The number of pores 2.3 nm in diameter increased considerably for the bottom ash treated in NaOH at 200 °C, where zeolite was the major phase. The main change in the pore size distribution introduced by washing was in the samples treated with NaOH, where the peak centered at 12 nm disappeared, showing a more homogeneous pore size distribution.

A general increase in the bottom ash surface area was produced under all of the treatments studied and especially those conducted in NaOH (Fig. 3), where the surface area increased

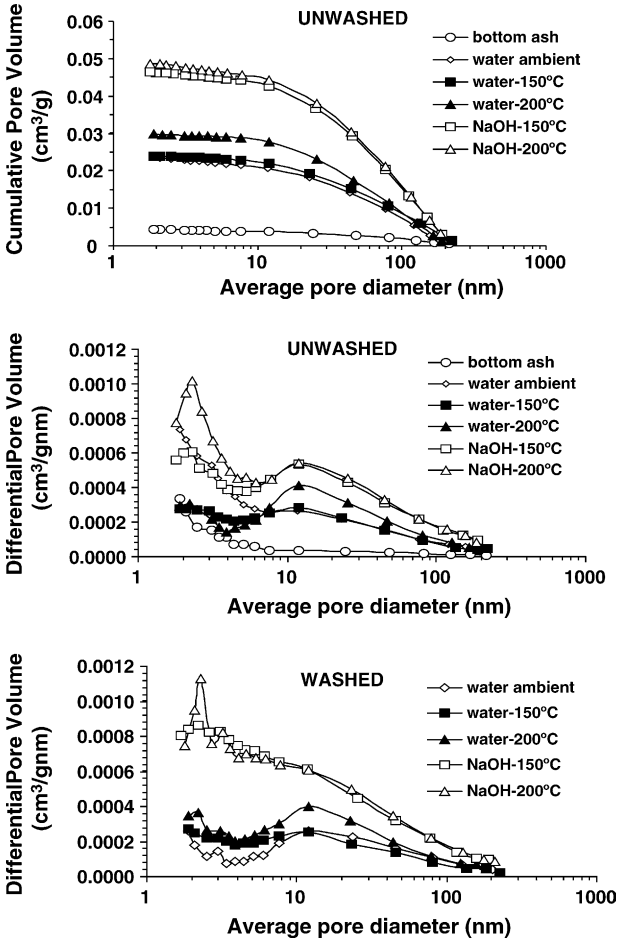

Fig. 2. Porosity and pore size distribution after the different bottom ash treatments: influence of washing.

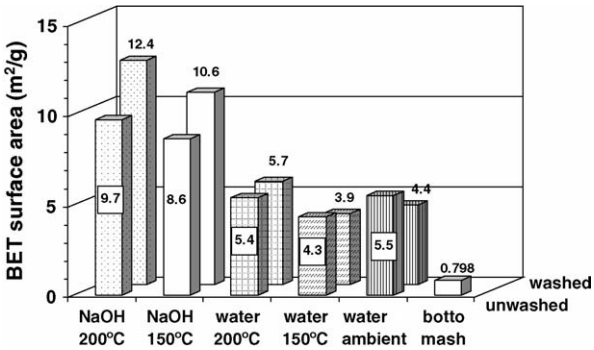

Fig. 3. BET-N_2 surface area after the different bottom ash treatments: influence of washing.

from 0.798 m^2/g for the untreated bottom ash to 8.6 and 9.7 m^2/g after HT at 150 and 200 °C, respectively. In the washed samples, a significant increase in the surface area was observed for the two aforementioned samples, whereas the rest of the samples remained almost unchanged.

3.1.3. Scanning electron microscopy analyses

SEM analyses were conducted on washed samples, after treatment in water at room temperature and at 200 °C (Figs. 4 and 5), and after treatment at 200 °C in NaOH (Fig. 6). The percentages of the main elements analyzed are given in Table 3. After treatment in water at room temperature (Fig. 4), numerous needles appeared, corresponding to ettringite, according to Al/Ca and S/Ca atomic ratio analysis (Figs. 4(a and b)), a result that justifies the increased BET surface area detected in Fig. 3. The aspect of the bottom ash changed with HT in water at 200 °C (Fig. 5), where the spherical particles of the bottom ash ("BA" in Fig. 5(a)) were covered with small plates of a composition consistent with that of scolecite ("S"). Under HT in Na(OH), the sample converted into aggregates of fine plates with a high sodium content, which could correspond to the zeolite detected by XRD. $Na_6[AlSiO_4]_6{\cdot}4H_2O$ (Si/Al and Na/Si = 1; "Z" in Fig. 6(a)), as well as tobermorite needles and small katoite rounded particles ("T" and "K" in Fig. 6(b)), were seen.

3.2. Retention study

Table 4 shows the concentration of cesium, cadmium, lead and chromium analyzed in the blanks and in the solutions filtered after 24 h, the percentages retained by the selected samples from the bottom ash transformation, and the distribution coefficient (K_d), defined as the ratio of the amount of element adsorbed per gram of sample to the amount of elements remaining in 1 ml of solution.

As shown in Table 4, the percentage of Cs^+ retained and the K_d value were considerably lower than those for Cd^{2+}, Pb^{2+} and Cr^{3+}, irrespective of the type of compounds formed under the different bottom ash treatments. The high percentage of retained Cs^+ (31%), with a distribution coefficient (K_d) of 222 ml/g, was reached after treatment of the bottom ash in NaOH at 200 °C, where the zeolite $Na_6[AlSiO_4]_6{\cdot}4H_2O$, massively formed together with aluminum tobermorite ($Ca_5Si_5Al(OH)O_{17}{\cdot}5H_2O$), so that the increase in retained Cs^+ could be attributed to

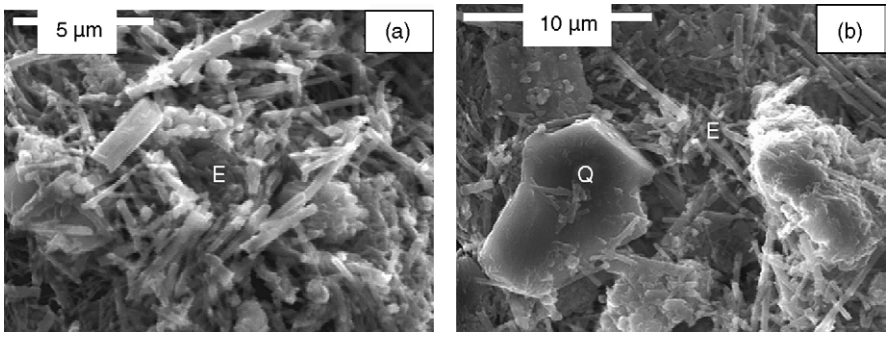

Fig. 4. SEM images of bottom ash (R1) after treatment in water at room temperature; needles of high S content, probably corresponding to ettringite (mark E in (a and b); big crystal of high Si content attributed to quartz (mark Q in (b)).

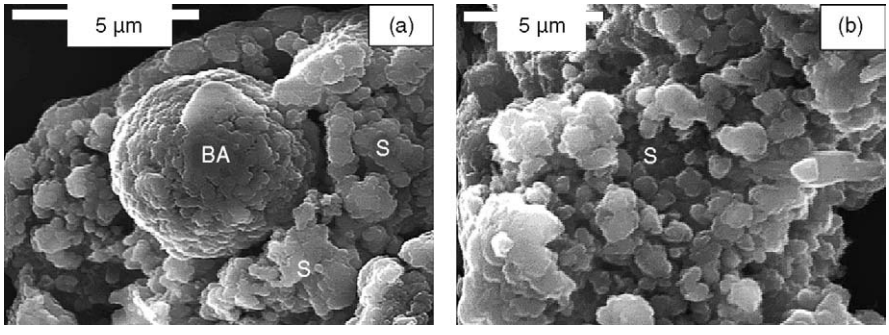

Fig. 5. SEM images of bottom ash (R1) after HT in water at 200 °C; spherical particle of bottom ash with rough surface (mark BA in (a)); plates of reacted bottom ash with composition consistent with scolecite (mark S in (a and b)).

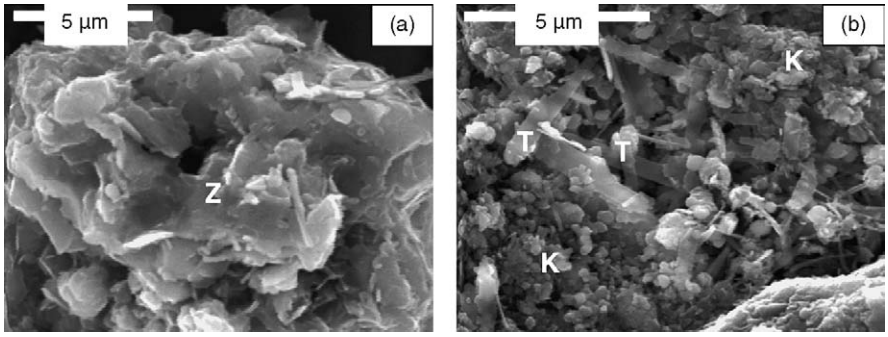

Fig. 6. SEM images of bottom ash (R1) after HT in NaOH at 200 °C: aggregate of zeolite plates (mark Z in (a)); small rounded particles of katoite particles (mark K in (b)); prismatic needles of tobermorite (mark T in (b)).

Table 3
X-ray microanalyses of bottom ash (R1) after different hydrothermal treatments (% atom)

	Si	Al	Ca	Mg	Na	K	Fe	S	Cl	Si/Ca	Al/Ca	Si/Al	S/Ca	Na/Si
Water-ambient														
Fig. 3(a) mark E	0.32	0.46	0.64	0 028	0.068	0.015	0.014	0.2	0.02	0.5	0.7	0.7	0.3	0.2
Fig. 3(b) mark E	0.48	0.46	0.55	–	0.064	0.037	0.004	0.145	0.037	0.9	0.8	1.0	0.3	0.1
Fig. 3(b) mark Q	1.5	0.02	0.076	0.001	0.033	0.006	–	0.019	0.005	19.7	0.3	75.0	0.3	0.0
HT-water-200 °C														
Fig. 4(a) mark BA	0.52	0.37	0.64	0.027	0.067	0.032	0.019	0.04	0.02	0.8	0.6	1.4	0.1	0.1
Fig. 4(a) mark S	0.67	0.54	0.41	–	0.089	0.027	0.013	0.029	0.025	1.6	1.3	1.2	0.1	0.1
Fig. 4(b) mark S	0.7	0.32	0.36	–	0.025	0.19	0.055	0.062	0.046	1.9	0.9	2.2	0.2	0.0
HT-NaOH-200 °C														
Fig. 5(a) mark Z	0.66	0.51	0.06	–	0.8	0.013	0.001	0.077	–	11.0	8.5	1.3	1.3	1.2
Fig. 5(b) mark T	0.56	0.38	0.66	–	0.15	0.04	0.01	0.006	0.001	0.8	0.6	1.5	0.0	0.3
Fig. 5(c) mark K	0.46	0.34	0.79	–	0.077	0.036	0.025	0.012	0.001	0.6	0.4	1.4	0.0	0.2

these compounds. The aluminum-substituted tobermorite synthesized by Yao et al. [15] through the HT of pretreated fly ash from the incineration of municipal waste showed a retention value for Cs^+ of 0.40 mmol/g. In our case, because of the mixture of zeolite and tobermorite, it was not possible to differentiate the real cation exchange properties for each compound.

In the case of Cd^{2+}, Pb^{2+} and Cr^{3+}, the percentage retained was ∼99% under all of the conditions studied and especially when the bottom ash was treated in NaOH at 150 °C, where the corresponding K_d values reached 3.66×10^5, 1.19×10^5 and 1.76×10^5 ml/g for Cd^{2+}, Pb^{2+} and Cr^{3+}, respectively.

To a better knowledge of the binding mechanism of these metals, it is important to know the pH of the solutions, which has a great influence on both the type of speciation and precipitation as hydroxides. One can try to approach this aspect by applying water chemistry models, in which the speciation as a function of pH, ionic strength, concentration of ions in solution and possible solids to be precipitated are taking into account.

For that, the pH values of the blanks and the solutions, measured after 24 h and the percentage of fraction precipitated of Cd, Pb and Cr (calculated according to the MINTEQ water chemistry model [21]) are presented in Table 5. As can be seen, the percentage of fraction precipitate as $Cd(OH)_2$, $Pb(OH)_2$ and $Cr(OH)_3$ is around 95% for Cd and almost 100% for Pb and Cr in a good agreement with the experimental results of Table 4.

The percentage distribution of hydrolysis products of the fraction dissolved obtained by applying the MINTEQ model in the pH range from 4 to 14 is presented in Fig. 7. In our experimental conditions, the pH of the solutions (Table 5) ranged from 9.6 to 10.5 in the case of Cd, from 9.1 to 10.2 for Pb and from 8.0 to

Table 4
Cs, Cd, Pb and Cr retained as a function of the bottom ash treatment

Treatment	(mol/l in solution)				Retained (%)				K_d (ml/g)			
	Cs	Cd	Pb	Cr	Cs	Cd	Pb	Cr	Cs	Cd	Pb	Cr
Blank	1.96×10^{-4}	9.79×10^{-5}	1.04×10^{-4}	6.77×10^{-5}								
Water-ambient	1.84×10^{-4}	5.34×10^{-7}	4.34×10^{-7}	7.79×10^{-7}	6	99.4	99.6	98.9	31	93786	119278	43087
Water-150 °C	1.81×10^{-4}	1.62×10^{-5}	1.40×10^{-6}	7.79×10^{-7}	8	83.7	98.7	98.9	42	2991	36672	43087
Water-200 °C	1.84×10^{-4}	5.78×10^{-7}	4.34×10^{-7}	9.33×10^{-7}	6	99.4	99.6	98.9	31	98806	119278	35896
NaOH-150 °C	1.81×10^{-4}	1.78×10^{-7}	4.34×10^{-7}	1.92×10^{-7}	8	99.8	99.6	99.7	42	366167	119278	176000
NaOH-200 °C	1.35×10^{-4}	5.78×10^{-6}	4.34×10^{-7}	6.83×10^{-7}	31	93.9	99.6	99.0	222	7962	119278	49466

Table 5
Percentage of fraction precipitated of Cd, Pb and Cr as a function of the pH of solutions, according to the MINTEQ computer model [21]

Treatment	Cd (%)	pH	Pb (%)	pH	Cr (%)	pH
Blank	0	5.1	0	5.2	0	4.8
Water-ambient	94.9	9.8	99.9	9.1	99.8	9.5
Water-150 °C	99.5	10.5	99.9	10.2	99.8	8.3
Water-200 °C	99.5	10.5	99.9	10.2	99.8	10.4
NaOH-150 °C	98.4	10.1	99.9	9.9	99.8	8.8
NaOH-200 °C	88.1	9.6	99.9	9.4	99.8	8.0

10.4 for Cr. All of these pH values favored the precipitation of species (see Fig. 7), and therefore, the main binding mechanism is precipitation.

Nevertheless, in our case, the solid phase is complex and cannot be introduced in this model, being difficult to distinguish the role played by solid phase in the high retention of Cd, Pb and Cr.

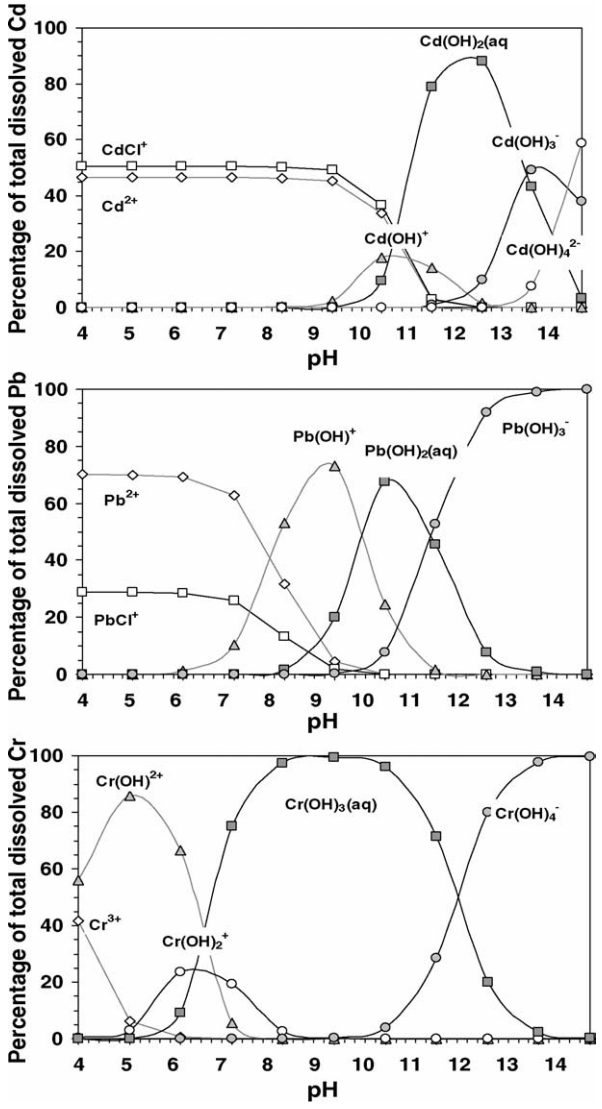

Fig. 7. Distribution of hydrolysis products at $I = 0.02$ m and 25 °C, of Cd(II) Pb(II) and Cr(III), according to the MINTEQ computer code [21].

It must be taken into account that all of the solid phase formed as a result of the hydrothermal treatment of bottom ash have potential retention properties. Andradite ($Ca_3Fe_2(SiO_4)_{3-x}(OH)_{4-x}$) and $Ca_3AlFe(SiO_4)(OH)_8$ have structures related to garnet ($Ca_3Al_2Si_3O_{12}$), with a cubic structure in which the Al^{3+} may be partly or wholly replaced by other divalent or trivalent cations, and Ca^{2+} may be replaced by monovalent cations [22].

C–S–H gel is a calcium silicate hydrate ($Ca_{1.5}SiO_{3.5}{\cdot}xH_2O$) with a layer structure very close to that of 14Å-tobermorite, it is the principal compound formed during the hydration of portland cement, being responsible for its mechanical strength gain. Like tobermorite, C–S–H gel can retain cations in the interlayer, such as cadmium [23], or anions, i.e., sulfate [24]. Katoite belongs to the structural family of hydrogarnet, having the aforementioned cation exchange properties.

Ettringite belongs to the AFt structural family, with anion and cation exchange properties. AFt (Al_2O_3–Fe_2O_3–tri) phases have the general formula $[Ca_3(Al,Fe)(OH)_6{\cdot}12H_2O]_2{\cdot}X_3{\cdot}xH_2O$, where $x \leq 2$ and X represents one formula unit of a double-charged or, with reservations, two formula units of a single-charged, anion. The term "tri" or "t" refers to the three units of CX in an alternative way of writing the formula, $C_3(A,F){\cdot}3CX{\cdot}yH_2O$ or $C_6(A,F)X_3{\cdot}yH_2O$, where $y = (x + 30)$. AFt phases form hexagonal prismatic or acicular crystals. The most important AFt phase is ettringite $[Ca_3Al(OH)_6{\cdot}12H_2O]_2{\cdot}(SO_4)_3{\cdot}2H_2O$, which is formed during the early hydration of portland cement [22]. Phases of the AFt-type also exist in which other cations replace the Ca^{2+} or Al^{3+} or both. Analogues with Fe^{3+}, Mn^{3+}, Cr^{3+} or Ti^{3+} in place of Al^{3+} also exist. Solid solution in the Fe^{3+}–Al^{3+} series is almost continuous [25].

4. Conclusions

- The major percentage of Cs^+ retained (31%), with a distribution coefficient (K_d) of 222 ml/g, was produced under HT of the bottom ash in NaOH at 200 °C. The binding retention mechanism is attributed to the cation exchange properties of the zeolite $Na_6[AlSiO_4]_6{\cdot}4H_2O$ and aluminum tobermorite ($Ca_5Si_5Al(OH)O_{17}{\cdot}5H_2O$).
- In the case of Cd^{2+}, Pb^{2+} and Cr^{3+}, the percentage retained was ~99% for all treatments of the bottom ash studied.
- According to the MINTEQ model, the mechanism of retention of Cd^{2+}, Pb^{2+} and Cr^{3+}, could be precipitation as the corresponding hydroxides.
- Evidence of the strong changes experienced by the bottom ash was manifested by the SEM, BET surface area and porosity results, with the major increases resulting for HT in the NaOH solution (1 order of magnitude, in both surface area and porosity).
- This transformation of the bottom ash from municipal solid waste incineration opens new opportunities for these type of residues in environmental waste disposal.

Acknowledgements

Funding for the present research was provided by the Scientific and Technological Research Commission (CICYT) under

Project PB98-0516. The authors wish to thank the Valdemingómez incinerator plant for the bottom ash supplied.

References

[1] P.J. Wainwright, P. Robery, Production and properties of sintered incinerator residues as aggregate for concrete, in: J.J.J.R. Goumans, H.A. Van der Sloot, Th.G. Aalbers (Eds.), Waste Materials in Construction, Elsevier Science Publishing Co., New York, 1991, pp. 425–432.
[2] J. Pera, L. Coutaz, J. Ambroise, M. Chababbet, Use of incinerator bottom ash in concrete, Cem. Concr. Res. 27 (1997) 1–5.
[3] M.T. Ali, W.F. Chang, Strength properties of cement stabilized municipal solid waste incinerator ash masonry bricks, ACI Mater. J. 91 (1994) 256–263.
[4] D.L. Gress, X. Zhang, S. Tarr, I. Pazienza, T.T. Eighmy, Municipal solid waste combustion ash as an aggregate substitute in asphaltic concrete, in: J.J.J.R. Goumans, H.A. Van der Sloot, Th.G. Aalbers (Eds.), Waste Materials in Construction, Elsevier Science Publishing Co., New York, 1991, pp. 161–175.
[5] D.J. Nonneman, F.A. Hansen, M.H.M. Coppens, The use of incinerator slag in asphalt for road construction, in: J.J.J.R. Goumans, H.A. Van der Sloot, Th.G. Aalbers (Eds.), Waste Materials in Construction, Elsevier Science Publishing Co., New York, 1991, pp. 569–578.
[6] C. Crignon, G. Pecqueur, E. Garcia Diaz, B. Germaneau, J.M. Siwak, Study of cement-treated MSWI bottom ash expansion, in: J. Méhu, G. Keck, A. Navarro (Eds.), Proceedings of the International Conference on Waste Stabilisation and Environment, Société Alpine de Publications, Grenoble, France, 1999, pp. 64–68.
[7] A. Nzihou, P. Sharrock, Extraction of chloride from fly ash and stabilisation of the residues by a hydroxylapatite sol–gel process, in: J. Méhu, G. Keck, A. Navarro (Eds.), Proceedings of the International Conference on Waste Stabilisation and Environment, Société Alpine de Publications, Grenoble, France, 1999, pp. 30–35.
[8] A. Guerrero, E. Fernández, A. Macías, S. Goñi, Hydrothermal treatment of fly ash from municipal solid waste incineration, in: G.R. Woolley, J.J.M. Goumans, P.J. Wainwright (Eds.), Proceedings of Waste Materials in Construction: Science and Engineering of Recycling for Environmental Protection, Pergamon, Amsterdam, 2000, pp. 178–185.
[9] A. Guerrero, S. Goñi, A. Macías, E. Fernández, Development of a low energy environmentally friendly cement, in: K. Dhir, R.D. Dyer, Thomas, J.E. Halliday (Eds.), Sustainable Concrete Construction, Proceedings of the International Conference on Challenges of Concrete Construction, Thomas Telford, Great Britain, 2002, pp. 95–106.
[10] A. Guerrero, S. Goñi, A. Macías, E. Fernández, Influence of synthesis temperature on the hydration of new cements from fly ash of municipal solid waste incineration, in: V.M. Malhotra (Ed.), Sustainable Development and Concrete Technology, Proceedings of CANMET/ACI International Symposium on Sustainable Development and Concrete Technology, vol. SP202, 2001, pp. 267–283.
[11] Y. Takuma, Y. Tsuchida, S. Uchida, Characteristics and hydration of cement produced from ash from incinerated urban garbage, in: H. Justnes (Ed.), Additives, Admixtures Characterisation Techniques, Proceedings of the 10th International Congress on the Chemistry of Cement, vol. 3, SINTEF, Tronheim Noruega, 1997, pp. 3ii118.
[12] H. Motzet, H. Pöllmann, The usage of alinite cement for waste stabilization, in: J.M. Cases, F. Thomas (Eds.), Proceedings of International Congress on Waste Solidification–Stabilization Processes, Société Alpine de Publications, Nancy, France, 1995, pp. 280–283.
[13] H. Takahashi, T. Maruta, K. Sakae, M. Kasahara, Application of water-washed incineration fly ashes as cement raw material, Muki Materiaru 5 (274) (1998) 200–207.
[14] M. Kasahara, H. Takahashi, K. Sakae, T. Maruta, Desalinizing of incineration ash and recycling as cement raw material by washing with water, Chichibu Onoda Kenkyu Hokoku 49 (2) (1998) 129–138.
[15] Z. Yao, C. Tamura, M. Matsuda, M. Miyake, Resource recovery of waste incineration fly ash: synthesis of tobermorite as ion exchanger, J. Mater. Res. 14 (1999) 4437–4442.
[16] M. Miyake, C. Tamura, M. Matsuda, Resource recovery of waste incineration fly ash: synthesis of zeolites A and P, J. Am. Ceram. Soc. 85 (7) (2002) 1873–1875.
[17] H. Teruo, S. Etsuro, Method of Producing Artificial Zeolite, Japanese Patent No. EP0963949, December 15, 1999.
[18] M. Janssen-Jurkovicova, G. Hollman Guido, Method for Preparing Zeolites from Fly Ash, European Patent No. WO9826101, June 18, 1998.
[19] R. Peña Penilla, A. Guerrero Bustos, S. Goñi Elizalde, Zeolite synthesized by alkaline hydrothermal treatment of bottom ash from combustion of municipal solid wastes, J. Am. Ceram. Soc. 86 (9) (2003) 1527–1533.
[20] W. Ma, P.W. Brown, S. Komarneni, Characterization and cation exchange properties of zeolites synthesized from fly ashes, J. Mater. Res. 13 (1998) 3–7.
[21] Equilibrium Speciation Model MINTEQ 4.02 provided by de US, Environmental Protection Agency (EPA), http://epa.gov/ceampubl/mmedia/minteq/index.htm.
[22] H.F.W. Taylor, in: H.F.W. Taylor (Ed.), Cement Chemistry, Academic Press, London, 1992.
[23] M.P. Pomiès, N. Lequeux, P. Boch, Speciation of cadmium in cement. Part I: Cd^{2+} uptake by C–S–H, Cem. Concr. Res. 31 (2001) 563.
[24] J.I. Escalante-García, J.H. Sharp, Variation in the composition of C–S–H gel in portland cement pastes cured at various temperatures, J. Am. Ceram. Soc. 82 (11) (1999) 3237–3241.
[25] H. Poellmann, St. Auer, H.J. Kuzel, R. Wenda, Solid solution of ettringites, Cem. Concr. Res. 23 (1993) 422–430.